C1q/TNF-related protein 9 alleviates atherosclerosis by inhibiting ox-LDL-induced VSMC-derived foam cell necroptosis via the AMPK pathway

Xuedong Wang[1], Xingtao Huang[1], Mengyue Yang[1], Lu Zhang[2], Ruoxi Zhang[2], Wenjuan Du[1], Jingbo Hou[1], and Qi Liu[1]

[1]Second Affiliated Hospital of Harbin Medical University
[2]The Key Laboratory of Myocardial Ischemia Organization, Chinese Ministry of Education

August 16, 2022

Abstract

Background and purpose: Necroptosis amplifies inflammation and plays an important role in atherosclerosis progression. However, the role of necroptosis of vascular smooth muscle cell (VSMC)-derived foam cells in atherosclerosis remains unknown. In the present study, we evaluated the effect of oxidized low-density lipoprotein (ox-LDL) on VSMC-derived foam cell necroptosis. Furthermore, we determined whether and how C1q/TNF-related protein 9 (CTRP9), a cardiovascular protective adipokine, protects against ox-LDL-induced cell dysfunction and atherosclerosis. Experimental approach: The VSMC-derived foam cell were established followed by incubation with ox-LDL and Tempol, CTRP9 and Compound C for 24 h. Cell death was detected by the mtROS levels and $\Delta\Psi$m, and the cellular inflammation was tested by the expression of inflammatory factors. Transmission electron microscopy and flow cytometry were used to confirm the occurrence of Necroptosis. Western blotting was used to detect the expression of necroptosis-related proteins and antioxidant enzymes. In vivo, adeno-associated virus (AAV) was used to construct an animal model of CTRP9 overexpression. Then the stability and necroptosis of aortic sinus plaque were detected. Key Results: Our results revealed that ox-LDL potently induced VSMC-derived foam cell necroptosis and promoted the expression of pro-atherosclerotic factors via an oxidative stress-related mechanism. CTRP9 significantly reversed ox-LDL-induced cell damage and the related dysfunction through the AMPK pathway-mediated expression of antioxidant enzymes. CTRP9 overexpression reduced atherosclerotic lesion size in the aortic sinus and enhanced features of plaque stability. Conclusions & Implications: Overall, our findings suggest that CTRP9 is a potential drug target to suppress atherosclerosis and stabilize plaques.

1. Introduction

Although primary and secondary preventive measures (especially statin and antiplatelet therapies) have reduced the risk of death due to cardiovascular diseases to a certain extent, cardiovascular diseases caused by atherosclerosis remain the main chronic diseases globally, with high mortality and disability rates, medical risks, and medical costs [1]. Thus, developing effective therapies remains a challenge in the management of millions of patients with atherosclerosis.

Growing evidence indicates that inflammation is a key regulator of atherosclerosis development and fragile plaque formation [2]. Cell death, especially necroptosis, is closely associated with inflammation. Lin et al. reported a large number of necroptotic cells and upregulated expression of receptor interacting protein kinase-3 (RIP3) in the necrotic core of progressive plaques [3]. Moreover, in human carotid plaques, the expression of necroptosis-related proteins such as RIP3 pseudokinase mixed lineage kinase domain-like (MLKL), and phosphorylated MLKL is upregulated [4]. Thus, cell necroptosis may be a promising target for the treatment

of atherosclerosis [5]. In addition, using both non-lineage and vascular smooth muscle cell (VSMC) lineage-tracing models, recent studies have shown that similar to human coronary atheromas, VSMCs contribute to the majority of cells in ApoE$^{-/-}$ mouse atherosclerosis plaques [6,7] and undergo various forms of cell death, typically lead to the formation of a lipid-rich necrotic core within the evolving intimal lesion. Therefore, regulating the death of VSMC-derived foam cells will provide clinical benefits. Multiple pathogenic factors associated with cardiovascular diseases can cause cell necroptosis. Oxidized low-density lipoprotein (ox-LDL), a major proatherogenic factor, exerts a proinflammatory effect [8] and is rich in plaque necrotic core. However, whether ox-LDL induces the necroptosis of VSMC-derived foam cell and enlargement of the necrotic core is unknown.

Ox-LDL causes reactive oxygen species (ROS) to accumulate abnormally in cells, and ROS are key targets in necroptosis regulation [9]. Therefore, we hypothesized that ROS may play an important role in ox-LDL-induced cell necroptosis. In our previous study, we found that C1q/TNF-related protein 9 (CTRP9) inhibits cholesterol-induced inflammatory cytokine secretion and monocyte adhesion in VSMCs by activating the AMPK pathway [10]. Activated AMPK can inhibit oxidative stress-induced mitochondrial dysfunction [11] and is essential to understand whether CTRP9 plays a protective role against ox-LDL-induced necroptosis in VSMC-derived foam cells and atherosclerosis. In this study, we aimed to evaluate the effect of ox-LDL on VSMC-derived foam cell necroptosis, determine the role of VSMC-derived foam cell necroptosis in inflammation, and examine whether and how CTRP9 protects against ox-LDL-induced cell dysfunction. Furthermore, we determined the effect of CTRP9 on atherosclerosis. Our study could help in understanding the initiation and development of atherosclerosis and a serve as a potential therapeutic target for atherosclerosis.

2. Materials and Methods

2.1. Cell Culture and VSMC-Derived Foam Cell Formation

Human aortic vascular smooth muscle cells (VSMCs, #6110) and smooth muscle cell medium (SMCM, 1101) were purchased from ScienCell (San Diego, CA, USA). VSMCs were cultured in SMCM containing 2% fetal bovine serum, 1% smooth muscle cell growth supplement (SMCGS), 100 units/mL penicillin, and 100 μg/mL streptomycin, at 37°C in a 5% CO_2 humidified atmosphere. VSMCs between passages three and six were used in all experiments. After reaching 70% confluence, VSMCs were synchronized in fetal bovine serum- and SMCGS-free SMCM and cultured at 37°C in a 5% CO_2 humidified atmosphere for 24 h. Cholesterol–methyl-β-cyclodextrin (C4951; Sigma, Saint Louis, MO, USA) was dissolved in SMCGS-free SMCM to a concentration of 5 μg/mL; the cell medium was replaced with this solution, and the cells were cultured for 72 h.

2.2. Cell Viability Assay using CCK8

Ox-LDL (YB-002; Yiyuan Biotechnologies, Guangzhou, Guangdong, China) was dissolved in SMCGS-free SMCM at different concentrations. VSMC-derived foam cells were treated with 0, 1, 10, and 100 μg/mL ox-LDL for 24 h. Next, 10 μL of CCK8 (Dojindo, Kumamoto, Japan) solution was added to each well and incubated for 2 h. The absorbance of the samples was measured at 450 nm using a Tecan Infinite M200 Microplate Reader (LabX, Austria). All experiments were performed in triplicate and repeated thrice.

2.3. CTRP9 Pre-Treatment of VSMCs

Recombinant human CTRP9 (R&D Systems, Minneapolis, MN, USA) was reconstituted at a concentration of 250 μg/mL in sterile PBS and diluted to different concentrations in SMCGS-free SMCM. After cell synchronization, VSMCs were incubated with fresh serum-free medium containing CTRP9 at the indicated concentrations such as 0.1, 1, and 10 μg/mL, and cultured for 30 min before ox-LDL treatment.

2.4. Measurement of Lactate Dehydrogenase Levels

The level of lactate dehydrogenase (LDH) released from the cells was measured using an LDH assay kit (A020; Nanjing Jiancheng Biology Engineering Institute, Nanjing, Jiangsu, China). VSMC-derived foam cells were treated with 0, 1, 10, and 100 μg/mL ox-LDL for 24 h. The cell supernatants were collected for

analysis. Matrix buffer, coenzyme I, and 2,4-dinitrophenylhydrazine solution were added to the samples, which were then incubated at 37°C for 15 min. The reaction was then terminated by adding an appropriate amount of 0.4 mol/L NaOH solution. The absorbance of the sample was determined at 450 nm using a microplate reader (LabX, Austria).

2.5. qRT-PCR

The total RNA was extracted using TRIzol reagent (Invitrogen, Carlsbad, CA, USA) according to the manufacturer's instructions. First-strand cDNA was generated from 4 μg of RNA using the Transcriptor First Strand cDNA Synthesis Kit (Roche, Penzberg, Germany). qRT-PCR was performed using FastStart Universal SYBR Green Master Mix (Roche, Penzberg, Germany) and a quantitative fluorescence PCR system (CFX96TMReal-Time System, Bio-Rad). Glyceraldehyde 3-phosphate dehydrogenase (*GAPDH*) or*β-actin* served as an internal control for mRNA quantification. Each sample was measured in triplicate. The qPCR data were analyzed, and mRNA expression normalized to GAPDH or β-actin expression was determined using the 2^{-Ct} cycle threshold method [12]. The related gene sequences were as follows: *MYH11* : forward 5'-AGATGGTTCTGAGGAGGAAACG-3, reverse 5'AAAACTGTAGAAAGTTGCTTATTCACT-3';*CD36* : forward 5'-CCAGTTGGAGACCTGCTTATC-3', reverse 5'-TCTGTAAACTTCTGTGCCTGTT-3'; *CD47* : forward 5'-AGATCCGGTGGTATGGATGAGA-3', reverse 5'-GTCACAATTAAACCAAGGCCAGTAG-3';*ICAM-1* : forward 5'-CCCCAACCCTTGATGATATG-3', reverse 5'-TAGTGCTTTTGTGCCGATAGA-3'; *VCAM-1* : forward 5'-AAATAATAAGCAAAGGGAGCACT-3', reverse 5'-CTGATGAACAAACTTCGTGAAAC-3';*IΛ-1β* : forward 5'-TCCCTGCCCACAGACCTT-3', reverse 5'-GCACATAAGCCTCGTTATCCC-3'; *IL-6* : forward 5'-ACTCACCTCTTCAGAACGAATTG-3', reverse 5'-CCATCTTTGGAAGGTTCAGGTTG-3';*IL-18* : forward 5'-TCTTCATTGACCAAGGAAATCGG-3', reverse 5'-TCCGGGGTG CATTATCTCTAC-3'; *MCP-1* : forward 5'-CAGCCAGATGCAATCAATGCC-3', reverse 5'-TGGAATCCTGAACCCACTTCT-3';*MMP9* : forward 5'-TGTACCGCTATGGTTACACTCG-3', reverse 5'-GGCAGGGACAGTTGCTTCT-3'; *PCSK9* : forward 5'-GGTGGAGGTGTATCTCCTAGA-3', reverse 5'-ACATTCTCGAAGTCGGTGAC-3';*GAPDH* : forward 5'-CCACTCCTCCACCTTTGAC-3', reverse 5'-ACCCTGTTGCTGTAGCCA-3'; and *β-actin* : forward 5'-CGTGGACATCCGCAAAGA-3', reverse 5'-GAAGGTGGACAGCGAGGC-3'.

2.6. JC-1

Mitochondrial membrane potential ([?]Ψm) was measured using the JC-1 mitochondrial membrane potential assay kit (Beyotime Institute of Biotechnology, Beijing, China). The cells were incubated with JC-1 working dye for 20 min, washed twice with cold JC-1 staining buffer, and visualized under a fluorescence microscope (DMI4000B; Leica, Wetzlar, Germany).

2.7. mtROS

The MitoSOX Red mitochondrial superoxide indicator (M36008; Invitrogen) was used to detect mitochondrial ROS (mtROS) accumulation. The cells were incubated with 1.0 mL of 5 μM MitoSOX reagent working solution for 10 min at 37°C in dark. Thereafter, the cells were washed gently with warm buffer thrice, and fluorescence was observed and photographed under a fluorescence microscope (DMI4000B; Leica, Wetzlar, Germany).

2.8. Transmission Electron Microscopy

Samples were fixed with 2.5% glutaraldehyde and 1% osmic acid overnight at 4°C for 1.5 h and then washed with phosphate-buffered saline (PBS) thrice for 15 min. The samples were dehydrated with different concentrations of gradient ethanol (30%, 50%, 70%, 80%, 90%, 95%, and 100%) and then embedded in a mixture of embedding agent and acetone at 70°C overnight. Subsequently, 70 nm-thick sections were obtained using a Reichert Jung ultrathin microtome and stained with lead citrate and uranyl acetate. The sections were observed under an H-7650 transmission electron microscope.

2.9. Flow Cytometry

After treatments, the cells were collected and stained with Annexin V/propidium iodide (PI) (BD Biosciences, Franklin Lakes, NJ, USA), washed twice with cold PBS, and then resuspended in 1× binding buffer at a concentration of 1×10^6 cells/mL. Next, 100 μL of the cell suspension was transferred to a 5 mL culture tube, and 5 μL of PE Annexin V and 5 μL of PI were added. The cells were gently vortexed and incubated for 15 min at 25°C in the dark, and 400 μL of 1× binding buffer was added to each tube. Flow cytometry analysis was performed using the FACSCanto II system equipped with BD FACSDiva software (Becton-Dickinson, San Jose, CA, USA). Based on the features of cell necroptosis, PI-positive cells were considered as the target cells.

2.10. Western Blotting

Briefly, equal amounts of total cell lysates were blotted onto polyvinylidene fluoride membranes, incubated with primary antibodies overnight at 4°C, washed, and incubated with peroxidase-conjugated secondary antibody for 1 h at 37°C. The primary antibodies against p-RIP1 (#65746), RIP1 (#33493), p-MLKL (#37333), MLKL (#14993), and SOD-2 (#13194s) were obtained from Cell Signaling Technology (Danvers, MA, USA). RIP3 (ab62344), GCLC (ab53179), Foxo3 (ab47285), GCLM (ab153967), HO1 (ab68477), and NQO1 (ab80588) were obtained from Abcam (Cambridge, MA, USA). The β-actin antibody (sc-47778) and peroxidase-conjugated goat anti-rabbit IgG or anti-mouse IgG were obtained from ZSGB-BIO (Beijing, China). Immuno-complexes were visualized on a luminescent imaging workstation (6600; Tanon, Shanghai, China), and electrochemiluminescence was detected with BeyoECL Plus (Beyotime Institute of Biotechnology, Beijing, China). Proteins were quantified using scanning densitometry with ImageJ software (National Institutes of Health, USA). Three independent experiments were performed.

2.11. Animal Procedures

ApoE-deficient ($ApoE^{-/-}$) mice with a C57BL/6J genetic background were provided by HFK Bioscience (Beijing, China). All mice were raised under specific-pathogen-free (SPF)-conditions and had free access to a standard purified mouse diet and water. All experiments were conducted in accordance with the institutional guidelines of Harbin Medical University. To observe the effect of CTRP9 on atherosclerosis in mice, 6-week-old male $ApoE^{-/-}$ mice were randomly divided into the following two groups: AAV-CTRP9 and AAV-control. The adeno-associated vector expressing CTRP9 and the negative control were synthesized by GenePharma (Shanghai GenePharma Co., Ltd., Shanghai, China). To deliver AAV, the mice were administered 10^{11} vector genome copies of AAV-CTRP9 or AAV-control via a single tail vein injection. Thereafter, the mice were fed a Western diet (21% fat and 1.25% cholesterol; Research Diets D12108C, New Brunswick, NJ, USA) for 8 weeks. After removing the adventitia and endothelium, the media of the aortic wall homogenates were used for western blotting. For histology, the aortic roots were embedded in OCT compound or paraffin, and then stored at -80 or room temperature until use.

2.13. HE staining

The aorta was fixed, dehydrated, and embedded with OCT before continuous sectioning using a frozen section machine (CryoStar NX70 HOMVPD, Thermo). Frozen sections were equilibrated at room temperature for 10min, stained with hematoxylin for 4min, and rinsed with running water for 10min; then stained with 1% eosin solution for 2min, and rinsed with running water for 30s. The sections were subjected to gradient alcohol for rapid dehydration, then cleared using xylene I, xylene II and xylene III for 5min, respectively. The sections were sealed with neutral resin and imaged by microscopy (Olympus,Tokyo, Japan).

2.14. Immunofluorescent Assay

Frozen sections were fixed and permeated at room temperature, then incubated with primary antibody against P16 (diluted in goat serum, 1:100) overnight at 4°C. Afterwards, the sections were flushed and incubated with fluorescent secondary antibody diluted with goat serum (1:200) at room temperature for 60 min in the dark. Finally, DAPI was used to stain the cell nucleus for 10 min. The sections were examined under a fluorescence microscope at 200x magnification (DMI4000B; Leica, Wetzlar, Germany).

2.15. Sirius Red staining

Paraffin sections were de-waxed and hydrated. The nuclei were stained with Weigert's hematoxylin for 8 minutes, and then washed in running water for 10 minutes. The slices were stained in picro sirius red for one hour and washed with acidified water twice. Physically remove most of the water from the slice by vigorous. The slices were dehydrated with 100% ethanol for three times, and finally transparented in xylene, and sealed with neutral gum. Images were taken using ordinary forward microscopy (Olympus, BX41).

2.16. Immunohistochemistry

For the immunohistochemistry of RIP3, the tissue were paraffin-coated and sectioned with a paraffin microtome at a thickness of 5 μm. Subsequently, the sections were dewaxed in xylene and hydrated in a gradient ethanol solution. After dewaxing, antigen recovery was performed in 10-mM sodium citrate buffer (pH 6.0) at 121°C for 15 min, followed by 3% methanolic hydrogen peroxide solution for 15 min to quench endogenous peroxidase activity. Then, the slides were treated with 0.3% Triton-X 100 to break the membrane for 15 min, and then washed with PBS for three times. The slides were incubated with primary antibody at 4 °C overnight. The next day, the slides were rewarmed for 10 min at RT and then incubated with secondary antibody at RT for 2 h and exposed to DAB chromogenic for 2-3 min. Finally, hematoxylin was used for staining cell nuclei for 5 min. At last, the final product was visualized using a microscopic imaging system.

2.17. Statistical Analysis

Data are expressed as mean ± standard deviation (SD). A one-way ANOVA followed by Student's t -test was used for multiple comparisons. Statistical significance was set at $p < 0.05$. Data were analyzed using GraphPad Prism software (GraphPad Inc., CA, USA).

3. Results

3.1. Ox-LDL Significantly Promotes VSMC-Derived Macrophage-Like Foam Cell Death

We evaluated the effects of different concentrations of ox-LDL on VSMC-derived macrophage-like foam cell death. VSMCs were established by treatment with 5 μg/mL cholesterol for 72 h, followed by incubation with different concentrations of ox-LDL for 24 h. Ox-LDL exerted a cell death-inducing effect at a relatively low concentration of 10 μg/mL (Fig. 1a and b). The Ox-LDL-treated cells also showed significant changes in the mtROS levels and $\Delta\Psi$m, in an ox-LDL dose-dependent manner (Fig. 1c and d). To further characterize the changes in cellular function, we performed qRT-PCR. The results showed that ox-LDL substantially increased the mRNA level of pro-atherosclerotic genes and inflammatory factors (CD36, CD47, ICAM-1, VCAM-1, IL-1β, IL-6, IL-18, MCP-1, MMP9, and PCSK9) (Fig. 1e) but significantly decreased the expression of the VSMC contraction phenotype marker MYH11 (Fig. 1e).

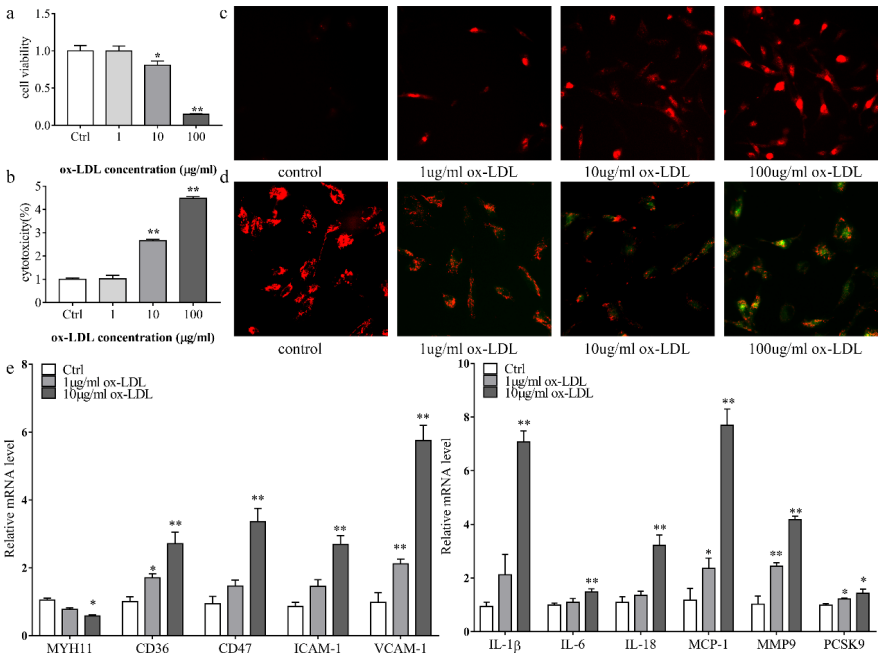

Figure 1: Ox-LDL induces VSMC-derived foam cell death, causes mtROS accumulation, reduces $\Delta\Psi$m, and upregulates pro-atherosclerosis factor expression. VSMCs were treated for 72 h with 5 μg/mL cyclodextrin-cholesterol complex to establish VSMC-derived foam cells, which were subsequently treated with different concentrations of ox-LDL for 24 h. (a) Viability of VSMC-derived foam cells was measured using the CCK8 assay. (b) LDH release was evaluated using a cytotoxicity detection kit. (c) Mitochondrial ROS levels were detected using the MitoSOX Red mitochondrial superoxide indicator after treating VSMC-derived foam cells for 6 h with different concentrations of ox-LDL. (d) A JC-1 staining kit was used to measure mitochondrial membrane potential after treating VSMC-derived foam cells for 6 h with different concentrations ox-LDL. (e) Real-time PCR analysis was performed to measure the mRNA levels of atherosclerosis-related factors, namely, MYH11, CD36, CD47, ICAM-1, VCAM-1, IL-1β, IL-18, MCP-1, MMP9, and PCSK9. Data are presented as mean ± SD of three independent experiments. *$p < 0.05$ vs. the control group; **$p < 0.01$ vs. the control group.

3.2. Οξ-ΛΔΛ (10 μγ/μΛ) Ινδυςες ΄ΣΜ΄-Δεριεδ Μαςροπηαγε-Λικε Φοαμ ἐλλ Necroptosis

Local inflammation in plaques plays an important role in atheroma progression. Because apoptotic and necroptotic cell death have distinct effects on inflammation, the type of cell death induced by ox-LDL needs to be determined. To illustrate the pattern of ox-LDL-induced cell death, cell morphology in each treatment group was examined using electron microscopy. The appearance of plasma membrane destruction and organelle fragmentation or swelling in 10 μg/mL ox-LDL-treated VSMC-derived macrophage-like foam cells revealed that the cells were necrotic (Fig. 2a). We used Annexin V and PI staining to determine the cell death rate (Fig. 2b). VSMC-derived macrophage-like foam cells without any treatment exhibited cell death, and PI-positive cells accounted for a major portion of these cells. As PI uptake is an indicator of the loss of cell membrane integrity, according to the feature of necroptosis cells, we calculated PI-positive cell rate and found that 10 μg/ mL ox-LDL treatment significantly promoted VSMC-derived macrophage-like foam cell necroptosis (Fig. 2c).

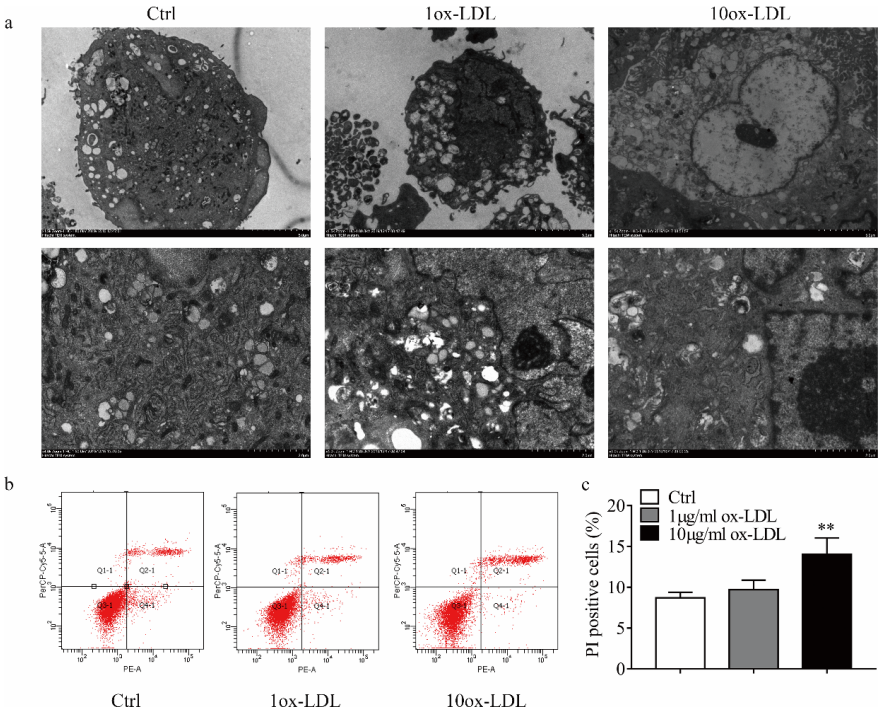

Figure 2: Ox-LDL (10 μg/mL) induces VSMC-derived macrophage-like foam cell necroptosis. VSMCs were treated for 72 h with 5 μg/mL cyclodextrin-cholesterol complex to establish VSMC-derived foam cells, which were subsequently treated with different concentrations of ox-LDL for 24 h. (a) The morphology of VSMC-derived foam cells was observed using transmission electron microscopy. (b) and (c) The proportion of PI-positive cells was determined using flow cytometry and analyzed quantitatively. Data are presented as mean ± SD of three independent experiments. **$p < 0.01$ vs. the control group.

3.3. Abnormal Accumulation of mtROS is Involved in VSMC-Derived Foam Cell Necroptosis

Phosphorylation of RIP1 and RIP3 is necessary for necroptosis activation. Han et al. reported that mtROS promoted RIP1 autophosphorylation and were essential for RIP3 recruitment into the necrosomes [9]. Other studies have illustrated that the mitochondrial permeability transition pore (mPTP) opening is essential for RIP3-mediated necroptosis [13,14], as it is a consequence of mitochondrial potential collapse. To elucidate the mechanism underlying ox-LDL-induced VSMC-derived foam cell necroptosis, we incubated VSMCs with an ROS scavenger, Tempol, before treatment with ox-LDL. After incubation with Tempol, the generation of mtROS induced by ox-LDL in VSMC-derived foam cells was reduced (Fig. 3a) and the loss of $\Delta\Psi m$ was also effectively inhibited (Fig. 3b). To further characterize the effect of Tempol on ox-LDL-induced cell necroptosis, the PI-positive cells were examined using flow cytometry. Following pre-incubation with Tempol, the number of ox-LDL-induced PI-positive cells was significantly reduced (Fig. 3c). These results suggest abnormal accumulation of mtROS as a potential mechanism underlying ox-LDL-induced cell necroptosis.

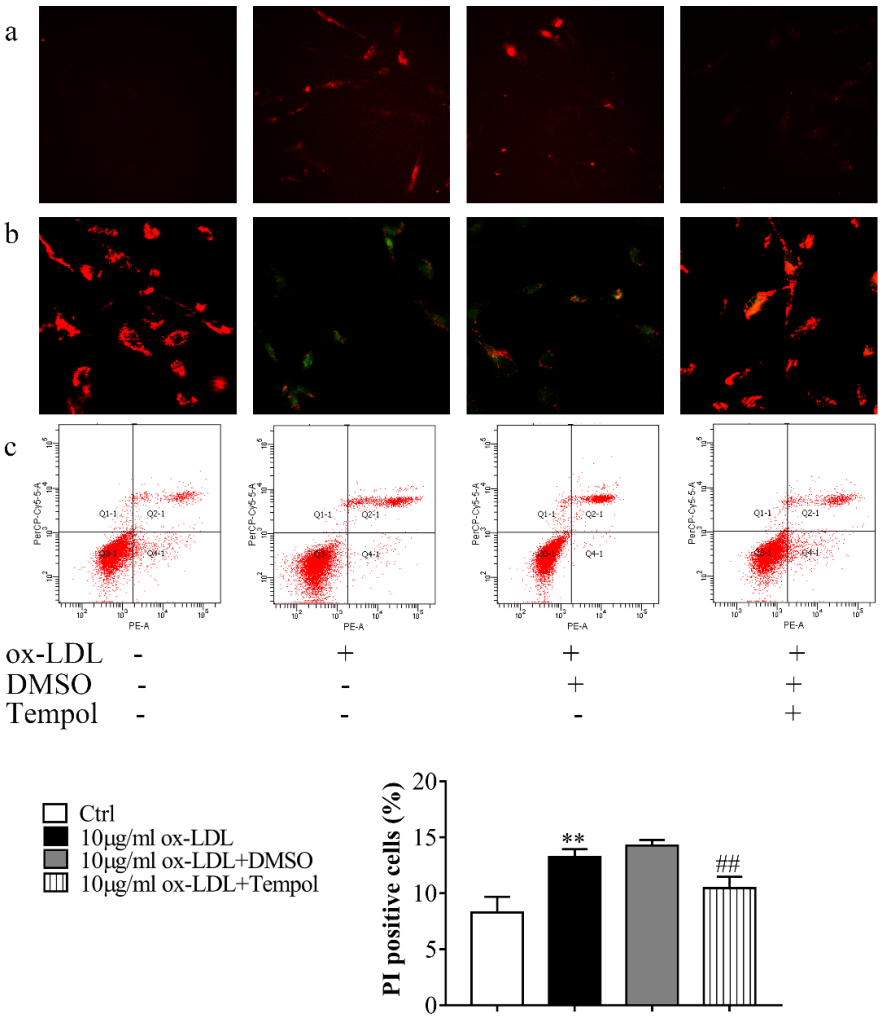

Figure 3. Abnormal accumulation of mtROS participates in ox-LDL-induced VSMC-derived foam cell necroptosis. Human aortic smooth muscle cells (HASMCs) were treated for 72 h with 5 μg/mL cyclodextrin-cholesterol complex to establish VSMCs, which were then subjected to DMSO, Tempol, and ox-LDL(10 μg/mL) treatment for 24 h. (a) mtROS levels were measured using a MitoSOX Red mitochondrial superoxide indicator. (b) A JC-1 staining kit was used to measure mitochondrial membrane potential. (c) The proportion of PI-positive cells was quantitatively determined using flow cytometry. Data are presented as mean ± SD of three independent experiments. **p < 0.01 vs. the control group; ##p < 0.01 vs. the 10 μg/mL ox-LDL group.

3.4. CTRP9 Alleviates ox-LDL-Induced VSMC-Derived Foam Cell Necroptosis

To clarify the potential role of CTRP9 in ox-LDL-induced necroptosis of VSMC-derived macrophage-like foam cells, we examined cell morphology using electron microscopy. VSMC-derived foam cells were either left untreated or treated with 10 μg/mL ox-LDL in the presence of different concentrations of CTRP9. With increasing CTRP9 concentration, the number of necroptotic cells decreased significantly, and the structure of the cell membrane and organelles became increasingly complete (Fig. 4a). In addition to altering cell morphology, CTRP9 reduced the proportion of PI-positive cells (Fig. 4b). Western blotting analysis revealed that ox-LDL promoted RIP1 and MLKL phosphorylation in VSMC-derived foam cells, whereas CTRP9 prevented this phosphorylation, and higher concentrations of CTRP9 further reduced the expression of

necroptosis-related proteins (Fig. 4c and d). Thus, CTRP9 effectively protected VSMC-derived foam cells from ox-LDL-induced necroptosis. To further verify this finding, we measured the expression levels of cell phenotype markers, pro-atherosclerotic genes, and inflammatory factors using qRT-PCR and found that CTRP9 inhibited the expression of pro-atherosclerotic genes and inflammatory factors induced by ox-LDL in a dose-dependent manner (Fig. 4e).

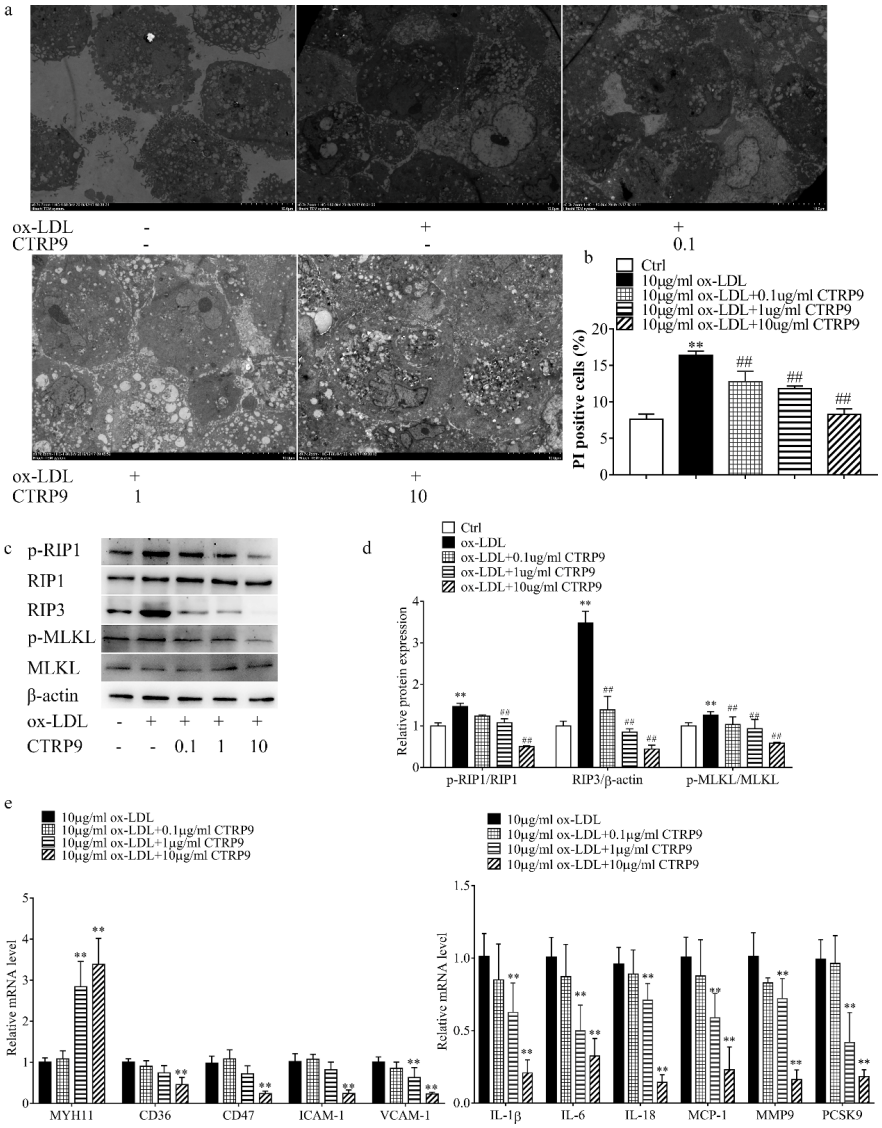

Figure 4. CTRP9 alleviates ox-LDL-induced VSMC-derived foam cell necroptosis. Human aortic smooth muscle cells (HASMCs) were treated for 72 h with 5 μg/mL cyclodextrin-cholesterol complex to establish VSMC-derived foam cells, which were subsequently exposed to different doses of CTRP9 (0–10 μg/mL) in the presence of ox-LDL (10 μg/mL) or left untreated (control) for 24 h. (a) The morphology of VSMC-derived foam cells was analyzed using transmission electron microscopy. (b) The proportion of PI-positive cells was determined quantitatively. (c) Western blotting was performed to examine the protein levels of MLKL, p-MLKL, RIP3, RIP1, and p-RIP1. (d) Quantitative analysis of necroptosis-associated protein expression. (e) Real-time PCR analysis of the mRNA levels of atherosclerosis-related factors. Data are presented as mean ± SD of three independent experiments. **$p < 0.01$ vs. the control group; ##$p < 0.01$ vs. the 10

μg/mL ox-LDL group.

3.5. CTRP9 Inhibits ox-LDL-Induced mtROS Accumulation by Regulating Antioxidant Enzyme Expression

To explore the mechanism by which CTRP9 alleviates ox-LDL-induced VSMC-derived foam cell necroptosis, we detected the changes in mtROS and ΔΨm in each treatment group. VSMC-derived foam cells were either left untreated or treated with 10 μg/mL ox-LDL in the presence of different concentrations of CTRP9. The results revealed that CTRP9 inhibited ox-LDL-induced production of mtROS and loss of ΔΨm in a dose-dependent manner (Fig. 5a and b). To elucidate the mechanism by which CTRP9 inhibits ox-LDL-induced necroptosis of VSMC-derived foam cells, we measured the level of antioxidant enzymes using western blotting. Interestingly, ox-LDL increased the expression of some antioxidant enzymes, such as Foxo3, HO1, SOD2, and NQO1, and pretreatment with CTRP9 increased the expression of these proteins to a higher degree than that in the ox-LDL-only group (Fig. 5c and d).

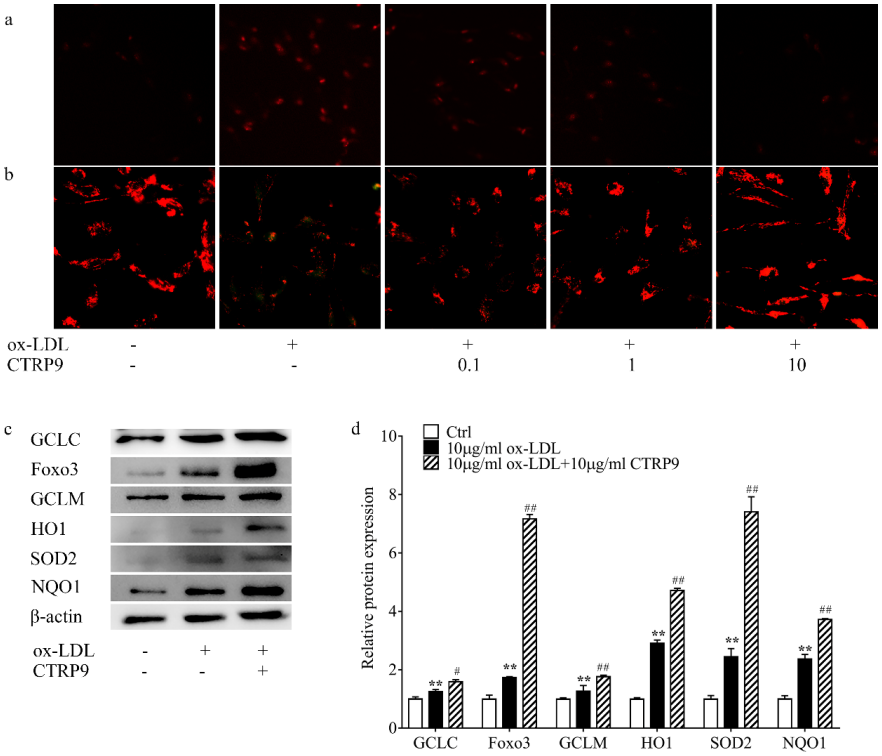

Figure 5. CTRP9 inhibits ox-LDL-induced mtROS accumulation by regulating antioxidant enzyme expression. Human aortic smooth muscle cells (HASMCs) were treated for 72 h with 5 μg/mL cyclodextrin-cholesterol complex to establish VSMC-derived foam cells, which were then incubated with different concentration of CTRP9 (0–10 μg/mL) in the presence of ox-LDL (10 μg/mL) or left untreated (control) for 24 h. (a) mtROS levels were measured using a MitoSOX Red mitochondrial superoxide indicator. (b) A JC-1 staining kit was used to detect mitochondrial membrane potential. (c) Western blotting was performed to examine the protein levels of GCLC, Foxo3, GCLM, HO1, SOD2, and NQO1. (d) Quantitative analysis of the expression of oxidant-related proteins. Data are presented as mean ± SD of three independent experiments. **$p < 0.01$ vs. the control group; #$p < 0.05$, ##$p < 0.01$ vs. the 10 μg/mL ox-LDL group.

3.6. Inhibition of the AMPK Pathway Abolishes the Protective Effect of CTRP9 on VSMC-Derived Foam Cells

Considering that CTRP9 is an agonist of the AMPK pathway, we aimed to further explore the role of AMPK

in the protective effect of CTRP9. To this end, the expression of antioxidant enzymes was measured after incubation with Compound C, a recognized inhibitor of the AMPK pathway. Pretreatment with Compound C notably decreased the expression of antioxidant enzymes, indicating that the AMPK pathway is essential for antioxidative enzyme expression (Fig. 6a and b). Pretreatment with Compound C significantly blocked the protective effect of CTRP9 against ox-LDL-induced VSMC-derived foam cell necroptosis, as revealed by the abnormal accumulation of mtROS and reduction in $\Delta\Psi$m (Fig. 6c and d). The effects of Compound C on the necrosomes were examined using western blotting. Inhibition of the AMPK pathway by Compound C promoted cell necroptosis, as evidenced by the increased phosphorylation of RIP1 and MLKL as well as the upregulated expression of RIP3 in VSMC-derived foam cells (Fig. 6e and f). Collectively, our findings suggest that CTRP9 inhibited ox-LDL-induced VSMC-derived foam cell necroptosis through the AMPK pathway.

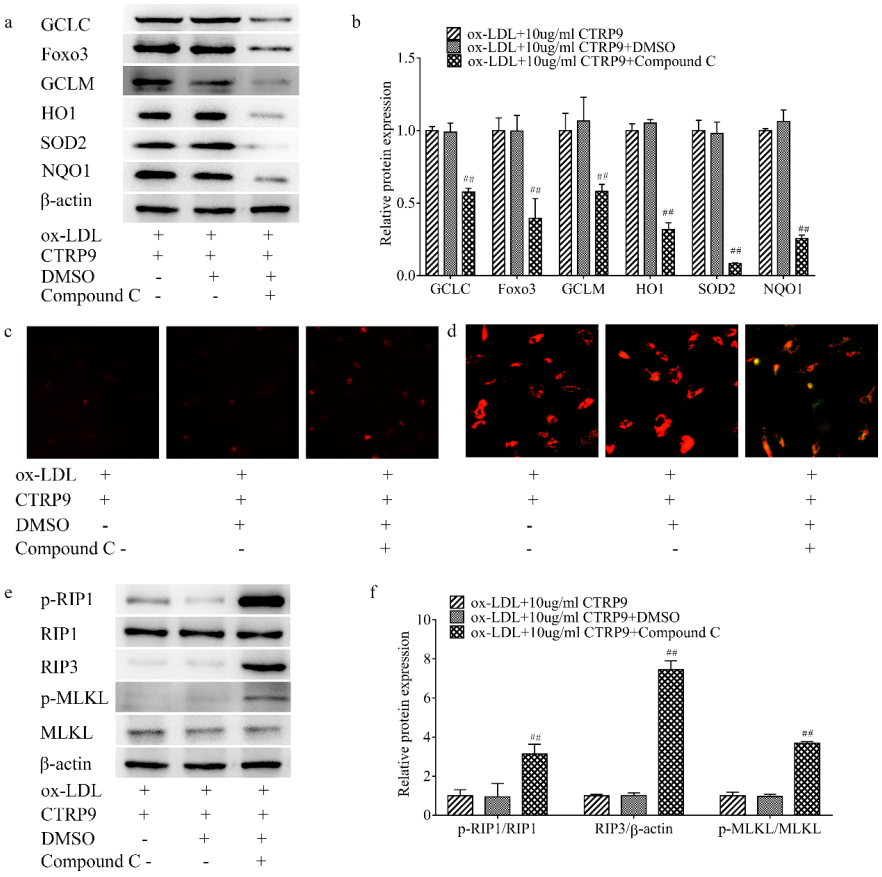

Figure 6. Inhibition of the AMPK pathway abolishes the protective effect of CTRP9 against VSMC-derived foam cell death. Human aortic smooth muscle cells (HASMCs) were treated for 72 h with 5 μg/mL cyclodextrin-cholesterol complex to establish VSMC-derived foam cells, which were then treated with CTRP9 (10 μg/mL) and ox-LDL (10 μg/mL) in the presence of Compound C or DMSO for 24 h. (a) Western blotting was performed to examine the protein levels of GCLC, Foxo3, GCLM, HO1, SOD2, and NQO1. (b) Quantitative analysis of the oxidant-related protein expression. (c) Mitochondrial ROS levels were detected using a MitoSOX Red mitochondrial superoxide indicator. (d) A JC-1 staining kit was used to detect mitochondrial membrane potential. (e) Western blotting was performed to examine the protein levels of MLKL, p-MLKL, RIP3, RIP1, and p-RIP1. (f) Quantitative analysis of necroptosis-associated protein expression. Data are presented as mean ± SD of three independent experiments. ##p < 0.01 vs. the ox-LDL + 10 μg/mL CTRP9 group.

3.7. CTRP9 Overexpression Enhances Features of Atherosclerotic Plaque Stability

In order to verify whether CTRP9 has a protective effect on atherosclerosis, adeno-associated virus was used to construct an animal model of CTRP9 overexpression. The western blotting result showed that compared with AAV-GFP, AAV-CTRP9 significantly increased CTRP9 expression in Apoe$^{-/-}$mice (Fig. 7e). To examine the effects of CTRP9 on atherosclerotic plaque stability, we first analyzed the lesion sizes using HE staining. Consistent with our previous study findings, CTRP9 reduced atherosclerotic plaque size (Fig. 7a). To determine whether CTRP9 overexpression influences the features of plaque stability or not, we performed Sirius Red staining to determine plaque collagen level. The plaque collagen level, which plays an important structural role in stabilizing plaques, was increased in CTRP9-overexpressed mice relative to that in the control mice (Fig. 7b). Additionally, the number of MYH11-positive cells was increased within plaques from CTRP9-overexpressing mice relative to those from the controls, and this is also consistent with increased plaque stability (Fig. 7c). Finally, the expression of RIP3 was significantly decreased in plaque in CTRP9-overexpressed mice relative to those from the control mice (Fig. 7d). Western blot was used to detect the expression of markers related to necroptosis in mouse aorta. The results showed that overexpression of CTRP9 significantly reduced the levels of p-RIP1, RIP3 and p-MLKL compared with the control group (Fig.7e and f), which indicates that the number of programmed necrotic cells in atherosclerotic plaque is significantly reduced. In addition, we also detected the expression levels of various inflammatory factors in the aorta. The results showed that the expression of inflammatory factors in the aorta of CTRP9-overexpressed mice was significantly decreased (Fig.7g). Overall, these results demonstrate that CTRP9 promotes features of a stable plaque phenotype in atherosclerosis.

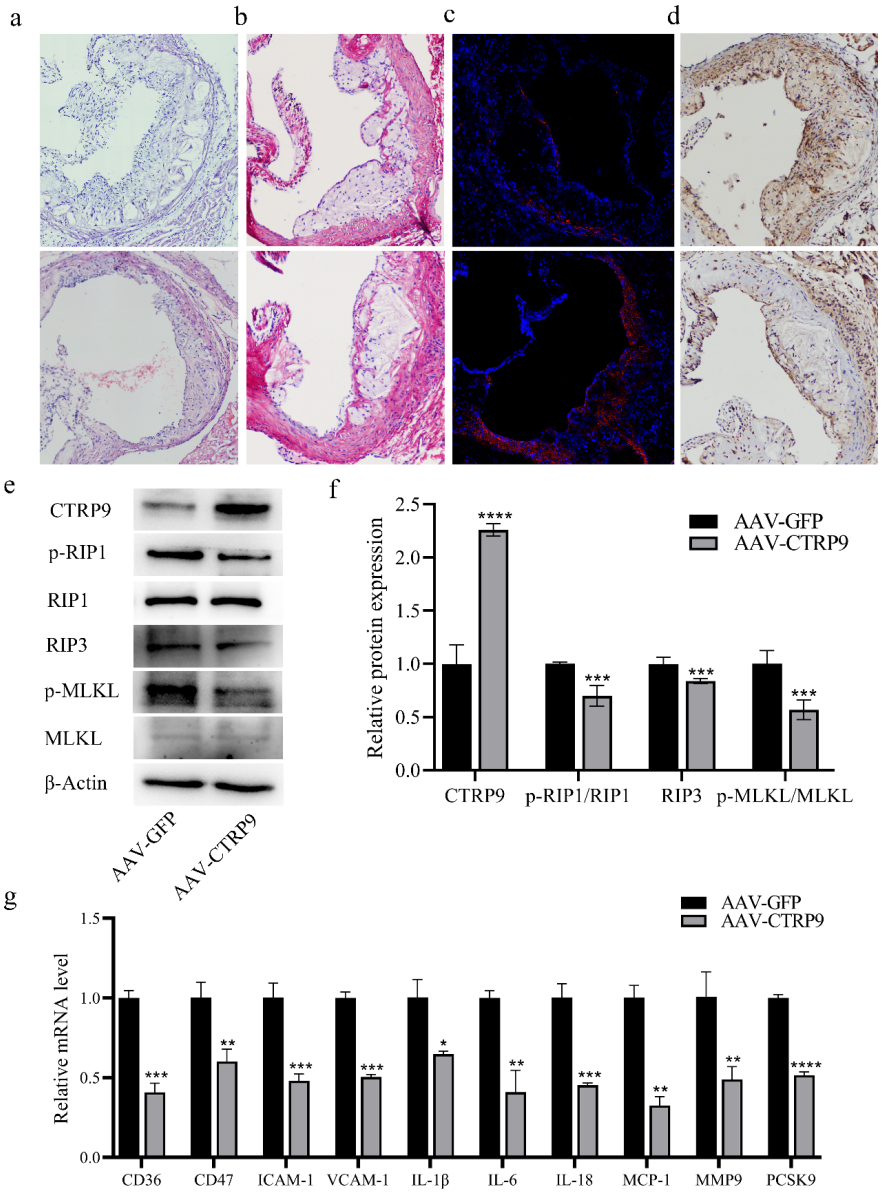

Figure 7. CTRP9 Overexpression Enhances Features of Atherosclerotic Plaque Stability. ApoE$^{-/-}$ mice were injected with AAV-CTRP9 and AAV-GFP (Control) through tail vein and fed a high-fat diet for 8 weeks. Representative images of the aortic root lesion area stained with HE (a) and Sirius Red (b). Immunofluorescence staining and Immunohistochemistry showing the expression of MYH11(c) and RIP3 (d) in atherosclerotic plaques. (e) Western blotting was performed to examine the protein levels of CTRP9, MLKL, p-MLKL, RIP3, RIP1 and p-RIP1. (f) Quantitative analysis of CTRP9 and necroptosis-associated protein expression. (g) Real-time PCR analysis of the mRNA levels of atherosclerosis-related inflammatory factors. Data are presented as mean ± SD of three independent experiments. *p < 0.05; **p < 0.01; *** p < 0.001; **** p < 0.0001 vs. the control group.

4. Discussion

The current study revealed, for the first time, that 10 μg/mL ox-LDL causes necroptosis in foam cells derived from VSMCs and that CTRP9 exerts a potent protective effect against ox-LDL-induced necroptosis. CTRP9

inhibited the formation of cell necrosomes and the subsequent inflammation in VSMCs pretreated with ox-LDL. Mechanistically, this effect is attributable to the upregulation of antioxidant enzymes due to AMPK activation in VSMC-derived foam cells. Importantly, CTRP9 overexpression significantly suppressed RIP3 and promoted the features of atherosclerotic plaque stability. These results imply that CTRP9 plays a protective role against atherosclerosis by regulating VSMC-derived foam cell necroptosis.

Ox-LDL acts as a danger-associated molecular pattern (DAMP) to stimulate the inflammatory activation of macrophages, VSMCs, and other surrounding cells [15]. In our study, ox-LDL potently induced cell necrosis and necroptosis in a dose-dependent manner at concentrations as low as 10 μg/mL. During the formation of atherosclerotic plaques, cellular turnover in the plaques becomes imbalanced as cells engraft lipids to form foam cells and undergo both apoptotic and nonapoptotic cell death [16]. Cell necroptosis leads to inefficient cell clearance, thus contributing to the acellular necrotic core. Cell necroptosis is characterized by the disruption of cellular membranes, release of massive intracellular contents, and expansion of the secondary inflammatory response, which may play a central role in plaque expansion. Therefore, considering that ox-LDL is abundantly present in plaques, our study provides a new perspective on the mechanism by which ox-LDL promotes plaque progression in atherosclerosis.

Necroptosis is closely associated with inflammation. We found that, consistent with the cellular characteristics of necroptosis, ox-LDL induced the secretion of proinflammatory cytokines such as IL-1β, IL-6, IL-18, and MCP-1. In addition, ox-LDL accelerated the expression of the macrophage marker CD36 and cell adhesion molecules. Interestingly, ox-LDL also induced the expression of CD47. CD47, known as the "do-not-eat-me" molecule, affects effective programmed cell removal and may lead to clonal expansion. Leeper et al. showed that VSMCs can produce hyperproliferative cells, which promote inflammation and escape immune surveillance, further leading to plaque expansion [6]. The pro-atherosclerosis factor TNF-α participates in the expression of CD47, which is upregulated in plaques [17]. In contrast, knockdown of the key antiphagocytic molecule CD47 suppressed the clonal expansion of SMCs in plaques *in vivo* [6]. CD47 expression in VSMC-derived foam cells after ox-LDL treatment may provide a clue to the potential mechanism underlying VSMC-derived foam cell accumulation in plaques and may represent a translational target for atherosclerosis treatment.

Oxidative stress response may be associated with ox-LDL-induced cell death [18,19], and a previous study has indicated that ROS overexpression induces necroptosis [20]. However, whether mtROS affect ox-LDL-induced necroptosis in VSMC-derived foam cells has not been reported. In this study, increased cell necroptosis accompanied by altered mtROS levels and $\Delta\Psi$m was observed in ox-LDL-treated VSMCs, but adding a ROS scavenger effectively reduced cell necroptosis. The results confirmed that oxidative stress was the basic mechanism underlying ox-LDL-induced cell necroptosis. We also revealed that CTRP9 exerted a strong antioxidant effect and that CTRP9 pretreatment prevented the abnormal accumulation of mtROS and inhibited cell necroptosis induced by ox-LDL. Consistent with our results, Zuo et al. also reported that CTRP9 restored the $\Delta\Psi$m and suppressed ROS generation [21]. Nevertheless, inhibition of the AMPK pathway in VSMC-derived foam cells by pretreatment with Compound C abolished the CTRP9-induced expression of antioxidant enzymes and downregulation of cell necroptosis-related proteins. These results indicate that AMPK activation is crucial for the protective effect of CTRP9 against ox-LDL-induced damage of VSMC-derived foam cells. Collectively, the findings of this study reveal the vital role of mtROS in ox-LDL-mediated necroptosis and the mechanism underlying the protective effect of CTRP9 against atherosclerosis.

RIP3 deficiency exerts athero-protective effects by reducing the lesion areas and plaque vulnerability [3,22]. Similarly, RIP1 inhibition via Nec-1 treatment reverses plaque maturation in $Apoe^{-/-}$ mice [4]. Knockdown of the necroptosis executioner MLKL decreases both programmed cell death and the necrotic core in plaques; however, the total lesion area remaines unchanged [16], suggesting that MLKL is associated with lipid accumulation in macrophages. In our study, we found that CTRP9 overexpression suppressed RIP3 expression in plaque and promoted the features of atherosclerotic plaque stability, suggesting that cell necroptosis is an effective target for atherosclerosis treatment. However, the therapies need to be carefully selected. For example, the advantage of RIP3 may be attributed to its function in regulating cytokine expression in VSMCs

through a cell death-independent mechanism [23]; thus, a target that can inhibit both cell necroptosis and inflammation factor expression can improve clinical benefits. CTRP9 has multiple functions, including exhibition of anti-inflammatory activity, prevention of oxidative damage, and inhibition of cell necroptosis. Therefore, CTRP9 may be a potential drug target in atherosclerosis.

5. Conclusions

In conclusion, our *in vitro* study revealed that CTRP9 inhibited ox-LDL-induced cell necroptosis and the subsequent inflammatory cytokine secretion. In vivo experiments, we also confirmed that CTRP9 is indeed effective in suppressing atherosclerosis and stabilizing plaques.

Author Contributions:

Conceptualization, Hou Jingbo. and Liu Qi; methodology, Wang Xuedong and Huang Xingtao.; software, Yang Mengyue; validation, Zhang Lu and Zhang Ruoxi.; formal analysis, Yang Mengyue.; writing—original draft preparation, Wang Xuedong and Huang Xingtao.; writing—review and editing, Du Wenjuan.; visualization, Liu Qi.; supervision, Hou Jingbo; All authors have read and agreed to the published version of the manuscript.

Funding: This research was funded by the National Natural Science Foundation of China, Grant No. 81970297 to Jingbo Hou, No. 81900309 to Qi Liu, and No. 82000330 to Xuedong Wang; the China Postdoctoral Science Foundation, Grant No. 2019M661306 to Qi Liu and No. 2018M640310 to Xingtao Huang; the Heilongjiang Postdoctoral Foundation, Grant No. LBH-Z18217 to Qi Liu and No. LBH-Z19032 to Xingtao Huang; and the Key Laboratory of Myocardial Ischemia Mechanism and Treatment (Harbin Medical University), Ministry of Education, Grant No. KF202017 to Qi Liu.

Data Availability Statement: The data used to support the findings of this study are available from the corresponding author upon request.

Conflicts of Interest: The authors declare no conflict of interest.

References

1. Libby, P.; Buring, J.E.; Badimon, L.; Hansson, G.K.; Deanfield, J.; Bittencourt, M.S.; Tokgözoğlu, L.; Lewis, E.F. Atherosclerosis.*Nat Rev Dis Primers* **2019,** *5* , 56.
2. Libby, P. Inflammation during the life cycle of the atherosclerotic plaque. *Cardiovasc Res* **2021,** *17* , 2525–2536.
3. Lin, J.; Li, H.; Yang, M.; Ren, J.; Huang, Z.; Han, F.; Huang, J.; Ma, J.; Zhang, D.; Zhang, Z.; Wu, J.; Huang, D.; Qiao, M.; Jin, G.; Wu, Q.; Huang, Y.; Du, J.; Han, J. A role of RIP3-mediated macrophage necrosis in atherosclerosis development. *Cell Rep***2013,** *3,* 200–210.
4. Karunakaran, D.; Geoffrion, M.; Wei, L.; Gan, W.; Richards, L.; Shangari, P.; DeKemp, E.M.; Beanlands, R.A.; Perisic, L.; Maegdefessel, L.; Hedin, U.; Sad, S.; Guo, L.; Kolodgie, F.D.; Virmani, R.; Ruddy, T.; Rayner, K.J. Targeting macrophage necroptosis for therapeutic and diagnostic interventions in atherosclerosis.*Sci Adv* **2016,** *2,* e1600224.
5. Gupta, K.; Phan, N.; Wang, Q.; Liu, B. Necroptosis in cardiovascular disease - a new therapeutic target. *J Mol Cell Cardiol***2018,** *118* , 26–35.
6. Wang, Y.; Nanda, V.; Direnzo, D.; Ye, J.; Xiao, S.; Kojima, Y.; Howe, K.L.; Jarr, K.U.; Flores, A.M.; Tsantilas, P.; Tsao, N.; Rao, A.; Newman, A.A.C.; Eberhard, A.V.; Priest, J.R.; Ruusalepp, A.; Pasterkamp, G.; Maegdefessel, L.; Miller, C.L.; Lind, L.; Koplev, S.; Björkegren, J.L.M.; Owens, G.K.; Ingelsson, E.; Weissman, I.L.; Leeper, N.J. Clonally expanding smooth muscle cells promote atherosclerosis by escaping efferocytosis and activating the complement cascade. *Proc Natl Acad Sci U S A* **2020,***117* , 15818–15826.
7. Chappell, J.; Harman, J.L.; Narasimhan, V.M.; Yu, H.; Foote, K.; Simons, B.D.; Bennett, M.R.; Jørgensen, H.F. Extensive Proliferation of a subset of differentiated, yet plastic, medial vascular smooth muscle cells contributes to neointimal formation in mouse injury and atherosclerosis models. *Circ Res* **2016,** *119* , 1313–1323.

8. Que, X.; Hung, M.Y.; Yeang, C.; Gonen, A.; Prohaska, T.A.; Sun, X.; Diehl, C.; Määttä, A.; Gaddis, D.E.; Bowden, K.; Pattison, J.; MacDonald, J.G.; Ylä-Herttuala, S.; Mellon, P.L.; Hedrick, C.C.; Ley, K.; Miller, Y.I.; Glass, C.K.; Peterson, K.L.; Binder, C.J.; Tsimikas, S.; Witztum, J.L. Oxidized phospholipids are proinflammatory and proatherogenic in hypercholesterolaemic mice. *Nature***2018,** *558* , 301–306.
9. Zhang, Y.; Su, S.S.; Zhao, S.; Yang, Z.; Zhong, C.Q.; Chen, X.; Cai, Q.; Yang, Z.H.; Huang, D.; Wu, R.; Han, J. RIP1 autophosphorylation is promoted by mitochondrial ROS and is essential for RIP3 recruitment into necrosome. *Nat Commun* **2017,** *8* , 14329.
10. Liu, Q.; Zhang, H.; Lin, J.; Zhang, R.; Chen, S.; Liu, W.; Sun, M.; Du, W.; Hou, J.; Yu, B. C1q/TNF-related protein 9 inhibits the cholesterol-induced Vascular smooth muscle cell phenotype switch and cell dysfunction by activating AMP-dependent kinase. *J Cell Mol Med* **2017,** *21* , 2823–2836.
11. Zeng, X.; Yang, J.; Hu, O.; Huang, J.; Ran, L.; Chen, M.; Zhang, Y.; Zhou, X.; Zhu, J.; Zhang, Q.; Yi, L.; Mi, M. Dihydromyricetin ameliorates nonalcoholic fatty liver disease by improving mitochondrial respiratory capacity and redox homeostasis through modulation of SIRT3 signaling. *Antioxid Redox Signal***2019,** *30* , 163–183.
12. Livak, K.J.; Schmittgen, T.D. Analysis of relative gene expression data using real-time quantitative PCR and the 2(-delta delta C(T)) method. *Methods* **2001,** *25* , 402–408.
13. Baines, C.P.; Kaiser, R.A.; Purcell, N.H.; Blair, N.S.; Osinska, H.; Hambleton, M.A.; Brunskill, E.W.; Sayen, M.R.; Gottlieb, R.A.; Dorn, G.W.; Robbins, J.; Molkentin, J.D. Loss of cyclophilin D reveals a critical role for mitochondrial permeability transition in cell death.*Nature* **2005,** *434* , 658–662.
14. Nakagawa, T.; Shimizu, S.; Watanabe, T.; Yamaguchi, O.; Otsu, K.; Yamagata, H.; Inohara, H.; Kubo, T.; Tsujimoto, Y. Cyclophilin D-dependent mitochondrial permeability transition regulates some necrotic but not apoptotic cell death. *Nature* **2005,***434* , 652–658.
15. Hartley, A.; Haskard, D.; Khamis, R. Oxidized LDL and anti-oxidized LDL antibodies in atherosclerosis - Novel insights and future directions in diagnosis and therapy. *Trends Cardiovasc Med***2019,** *29* , 22–26.
16. Rasheed, A.; Robichaud, S.; Nguyen, M.A.; Geoffrion, M.; Wyatt, H.; Cottee, M.L.; Dennison, T.; Pietrangelo, A.; Lee, R.; Lagace, T.A.; Ouimet, M.; Rayner, K.J. Loss of MLKL (mixed lineage kinase domain-like protein) decreases necrotic core but increases macrophage lipid accumulation in atherosclerosis. *Arterioscler Thromb Vasc Biol* **2020,** *40* , 1155–1167.
17. Kojima, Y.; Volkmer, J.P.; McKenna, K.; Civelek, M.; Lusis, A.J.; Miller, C.L.; Direnzo, D.; Nanda, V.; Ye, J.; Connolly, A.J.; Schadt, E.E.; Quertermous, T.; Betancur, P.; Maegdefessel, L.; Matic, L.P.; Hedin, U.; Weissman, I.L.; Leeper, N.J. CD47-blocking antibodies restore phagocytosis and prevent atherosclerosis. *Nature***2016,** *536* , 86–90.
18. Cui, S.; Lv, X.; Li, W.; Li, Z.; Liu, H.; Gao, Y.; Huang, G. Folic acid modulates VPO1 DNA methylation levels and alleviates oxidative stress-induced apoptosis in vivo and in vitro. *RedoxBiol* **2018,** *19* , 81–91.
19. Xin, T.; Lu, C.; Zhang, J.; Wen, J.; Yan, S.; Li, C.; Zhang, F.; Zhang, J. Oxidized LDL disrupts metabolism and inhibits macrophage survival by activating a miR-9/Drp1/mitochondrial fission signaling pathway. *Oxid Med Cell Longev* **2020,** *2020* , 8848930.
20. Yang, Z.; Wang, Y.; Zhang, Y.; He, X.; Zhong, C.Q.; Ni, H.; Chen, X.; Liang, Y.; Wu, J.; Zhao, S.; Zhou, D.; Han, J. RIP3 targets pyruvate dehydrogenase complex to increase aerobic respiration in TNF-induced necroptosis. *Nat Cell Biol* **2018,** *20* , 186-197.
21. Zuo, A.; Li, J.; Zhao, X.; Li, T.; Lei, S.; Chen, J.; Xu, D.; Song, C.; Li, N.; Ruan, S.; Lyu, L; Guo, Y. Globular CTRP9 protects cardiomyocytes from palmitic acid-induced oxidative stress by enhancing autophagic flux. *Chem-Biol Interact* **2020,***329* , 109094.
22. Meng, L.; Jin, W.; Wang, X. RIP3-mediated necrotic cell death accelerates systematic inflammation and mortality. *Proc Natl Acad Sci U S A* **2015,** *112* , 11007–11012.
23. Wang, Q.; Liu, Z.; Ren, J.; Morgan, S.; Assa, C.; Liu, B. Receptor-interacting protein kinase 3 contributes to abdominal aortic aneurysms via smooth muscle cell necrosis and inflammation.*Circ Res* **2015,** *116* , 600–611.